Statistical properties of homogenized random polycrystals with uncertain single crystal elastic moduli

N. Sheng[1], S. Khazaie [1], M. Chevreuil[1], S. Fréour [1]

[1] *Institut de Recherche en Génie Civil et Mécanique (GeM – UMR CNRS 6183), Nantes Université, France, {ningyue.sheng @univ-nantes.fr}*

Résumé — Effective properties of polycrystals are often estimated by taking into account solely the intrinsic variabilities in crystallographic orientations along with those of the morphological shapes of the grains. The variability on the single crystal elastic moduli is not considered. In this work, we calculated the analytical estimates for effective elastic moduli of numerically generated equiaxed cubic polycrystals. The influence of the variability of the components of the single crystal elasticity tensor on the statistical properties of the homogenized macroscopic stiffness tensor is investigated.

Mots clés — Polycrystals, effective elastic moduli, variability of elasticity tensor

1. Introduction

Polycrystals are composed of many crystallites or grains with varying size and orientation whose apparent mechanical properties are often of interest. The different crystallographic orientations and the spatial morphology of grains in polycrystals ultimately determine most of the effective mechanical properties at macroscopic scale. In most theoretical and numerical works related to the effective properties of polycrystals, these two inherent variabilities are often considered by introducing the randomness on the grain orientations and their morphological texture. For a given phase, the single crystal elastic properties of each grain are assumed to be constant and deterministic in the reference frame of the grain. However, the local stiffness tensor is not constant and has variabilities. For instance, several studies reported different values for the components of the elasticity tensor of α-Fe monocrystals [1, 5, 7, 12, 15, 18, 21]. This variability on the local stiffness tensor may come from the changeability of the distribution of the addition elements in different grains, which results in a significantly non-uniform chemical composition of the grains (from one grain to another). Numerical models introduce these variabilities as randomness introduced on the elasticity matrix (for more details see C. Soize [19] and references therein). The uncertainty on the elasticity tensor of the individual grains and its influence on the statistical properties of the homogenized stiffness tensor of polycrystalline materials being unexplored, it will be the main focus of this work.

In this study, we will present a method to construct numerical models of polycrystals by introducing the variabilities both on the elastic moduli of grains and on the crystallographic orientations based on the experimental electron backscatter diffraction (EBSD) data. This method will be introduced in Sec. 2. Sec. 3 discusses the self-consistent method to estimate the effective elastic properties. Finally, the results are shown and discussed in Sec. 4.

2. Numerical model for simulation of polycrystals

2.1. Numerical simulation of random elasticity tensors

The fourth-rank elasticity tensor of a cubic medium is composed of three independent parameters c_{11}, c_{12} and c_{44} on a single crystal scale. It could be decomposed as a linear combination of three linearly independent tensors $\mathbb{P}$, $\mathbb{Q}$, $\mathbb{W}$ and three positive eigenvalues $\lambda_1, \lambda_2, \lambda_3$:

$$\mathbb{C}^{\text{cubic}} = \lambda_1 \mathbb{P} + \lambda_2 \mathbb{Q} + \lambda_3 \mathbb{W}. \tag{1}$$

The eigenvalues $(\lambda_1, \lambda_2, \lambda_3)$ with multiplicities of 1, 3 and 2 are linked to the elastic moduli as:

$$\lambda_1 = c_{11} + 2c_{12}, \qquad \lambda_2 = c_{44}, \qquad \lambda_3 = c_{11} - c_{12}. \tag{2}$$

The fourth-rank tensors $\mathbb{P}$, $\mathbb{Q}$ and $\mathbb{W}$ are mutually orthogonal. The definitions of them in terms of the crystallographic directions of a cubic medium can be found in [14].

Following Guilleminot and Soize [6] and based on the maximum entropy principle, the eigenvalues in the tensor decomposition of Eq. (1) are statistically independent gamma-distributed random variables. We assume that the coefficient of variation of λ_2 be δ (*i.e.*, $\delta_{\lambda_2} = \delta$), then for other two eigenvalues we get $\delta_{\lambda_1} = \sqrt{3\delta^2/(1+2\delta^2)}$ and $\delta_{\lambda_3} = \sqrt{3\delta^2/(2+\delta^2)}$, respectively. The Gamma marginal probability density functions (PDFs) of these independent eigenvalues can be written in terms of the dispersion level δ and the average elastic moduli ($\underline{c}_{11}, \underline{c}_{12}, \underline{c}_{44}$) as:

$$\lambda_1 \sim G\left(\frac{1+2\delta^2}{3\delta^2}, \frac{3(\underline{c}_{11} + 2\underline{c}_{12})\delta^2}{1+2\delta^2}\right); \quad \lambda_2 \sim G\left(\frac{1}{\delta^2}, \underline{c}_{44}\delta^2\right); \quad \lambda_3 \sim G\left(\frac{2+\delta^2}{3\delta^2}, \frac{3(\underline{c}_{11} - \underline{c}_{12})\delta^2}{2+\delta^2}\right). \tag{3}$$

Random elasticity tensors of cubic media $\mathbb{C}^{\text{cubic}}$ could be generated according to tensor decomposition (Eq. 1) and their fluctuation level could be defined by a single parameter δ. Based on different experimental estimations of the elastic moduli of α-Fe monocrystals reported in [1, 5, 7, 12, 15, 18, 21], the coefficient of variation of shear modulus is estimated as $\delta = 0.03$. For our numerical investigations, due to the lack of the experimental dataset, we assume the maximum value of δ to be nearly three times of our estimated value. Thus, we chose the values of δ on the interval $[0, 0.1]$. The mean values of $\underline{c}_{11}, \underline{c}_{12}$ and $\underline{c}_{44}$ are given in Table 1 for our studied materials. Fig. 1 shows the PDFs of components c_{11}, c_{12} and c_{44} of the random elasticity tensor $\mathbb{C}^{\text{cubic}}$ for α-Fe with three different fluctuation levels, $\delta \in \{0.005, 0.05, 0.1\}$. As expected, larger values of δ increase the variance of the corresponding distributions.

Table 1 – Average values of single crystal elastic moduli (GPa) and anisotropy index A for nine cubic materials [4, 10].

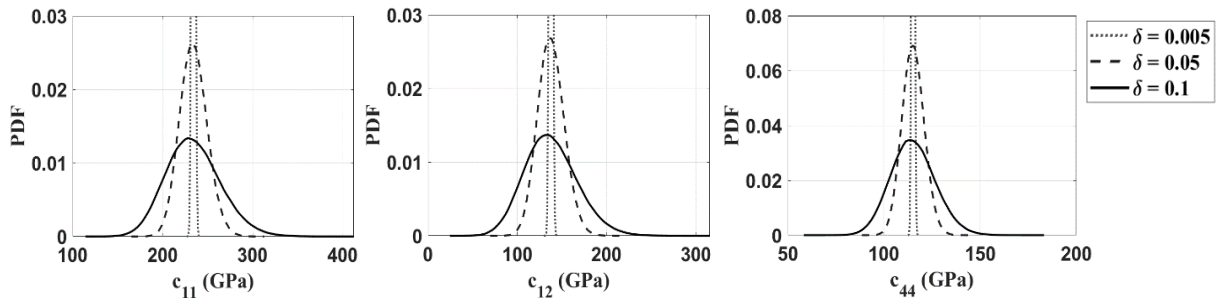| Name	Al	Pt	α-Fe	Ni	Au	Cu	K	Na	Li
$\underline{c}_{11}$	108	347	234.2	247	191	169.68	3.71	7.39	13.5
$\underline{c}_{12}$	62	251	137.7	153	162	122.55	3.15	6.22	11.44
$\underline{c}_{44}$	28.3	76.5	115.1	122	42.2	74.49	1.88	4.19	8.78
A	0.23	0.59	1.39	1.60	1.91	2.16	5.71	6.16	7.52

Figure 1 – PDFs of the components c_{11} (left), c_{12} (middle) and c_{44} (right) of numerically generated elasticity tensor $\mathbb{C}^{\text{cubic}}$ for α-Fe with different fluctuation levels δ.

2.2. Numerical simulation of random crystallographic orientations

In Sec. 2.1, we generated random elasticity tensors with a given fluctuation level δ for a single crystal in its local coordinates. Using the so-called Bond transformation matrix, one can transform the stiffness matrix C^{local} in local coordinates into C^{global} in polycrystalline global reference via:

$$C^{global}(\delta) = M C^{local}(\delta) M^{T}. \tag{4}$$

We subsequently aim at generating the Euler angles random fields based on a real sample. The microstructural map of this sample is deduced from EBSD technique by using experimental data from G. Doumenc [2], which is displayed in Fig. 2. The PDFs of the Euler angles $(\Theta_1, \Theta, \Theta_2)$ in Fig. 2 clearly show they have a non-Gaussian probabilistic content. According to our estimation, the two-point normalized auto-correlation function (NACF) of the random Euler angles of this sample follows an exponential form as:

$$\widehat{R}_{XX}(\eta) = \exp\left(-\frac{\eta}{l_X}\right), \qquad X \in (\Theta_1, \Theta, \Theta_2), \tag{5}$$

with $l_X = (l_{\Theta_1}, l_\Theta, l_{\Theta_2}) \cong (5.525, 6.452, 6.452)$ μm being the correlation lengths and η the distance between any two points. The exponential fit for the estimated $\widehat{R}_{\Theta_1\Theta_1}$ is shown in Fig. 2. Thus, the $N_g \times N_g$ normalized auto-correlation matrices for N_g grains can be expressed as:

$$\widehat{R}_{XX}(\mathbf{x}_m, \mathbf{x}_n) = \exp\left(-\frac{1}{l_X}\|\mathbf{x}_m - \mathbf{x}_n\|\right), \qquad m, n = 1, \dots, N_g, \qquad X \in (\Theta_1, \Theta, \Theta_2), \tag{6}$$

where $\mathbf{x}_m$ and $\mathbf{x}_n$ are spatial positions of the centroids of any two grains, l_X are the corresponding correlation lengths. The two-point normalized cross-correlation functions (NCCF) of the random Euler angles of this sample are 0, implying that different Euler angles are decorrelated.
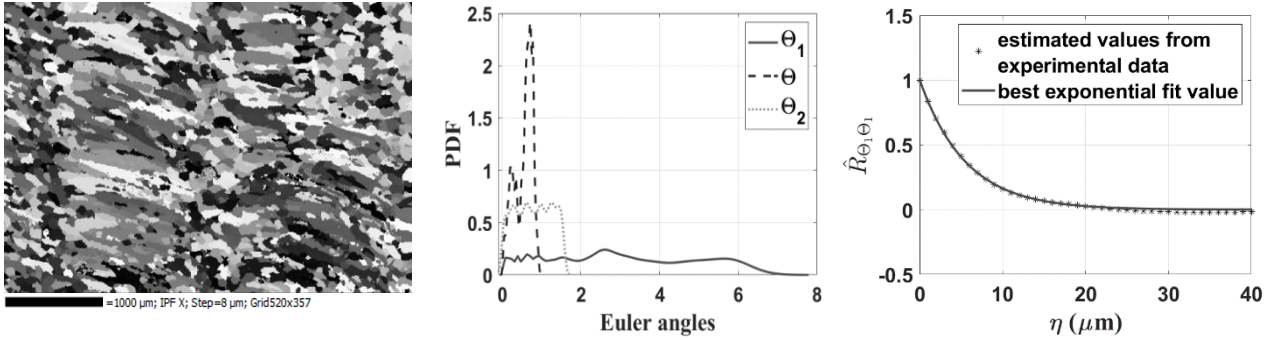

Figure 2 – Microstructural EBSD map of a real sample (left), with its PDFs of Euler angles $(\Theta_1, \Theta, \Theta_2)$ (middle) and the best fit for the NACF $\widehat{R}_{\Theta_1\Theta_1}$ (right).

The simulation of a desired non-Gaussian process can be performed by first generating a standard Gaussian process with an appropriate target covariance function. A Gaussian random field $\mathbf{Z}$ can be represented as a Karhunen-Loève (K-L) series expansion [11, 20] since K-L expansion is the most efficient method for representing the random process if the exact eigenvalues and eigenfunctions of the covariance function can be found:

$$\mathbf{Z}(\mathbf{x}, \vartheta) \cong \sum_{i=1}^{N_g} \sqrt{\alpha_i} \beta_i(\mathbf{x}) \gamma_i(\vartheta), \tag{7}$$

where N_g is the number of grains, $\mathbf{x}$ is the spatial position being the centroid of each grain, $\{\gamma_i(\vartheta)\}$ is a set of uncorrelated standard Gaussian random variables, α_i are eigenvalues and $\beta_i(\mathbf{x})$ are $\mathbb{R}^3$-valued eigenvectors of the covariance matrix $[R_{XX}(\mathbf{x}_m, \mathbf{x}_n)]$.

3

Using the so-called inverse transform sampling technique, one can transform the random field of Eq. (7) to a random field having a different marginal PDF. The corresponding spatially correlated Euler angles for one crystal can thus be generated as the following transformation:

$$x_X^n = F_X^{-1}\left(\Phi\left(\mathbf{Z}_X(\mathbf{x}_n)\right)\right), \quad X \in (\Theta_1, \Theta, \Theta_2), \quad n = 1, \dots, N_g, \tag{8}$$

in which $\mathbf{Z}_X(\mathbf{x}_n)$ is zero mean unit-variance component of an $\mathbb{R}^3$-valued Gaussian random field that we generated by using Eq. (7), $\mathbf{Z}_X(\mathbf{x}_n) = \left(\mathbf{Z}_{\Theta_1}(\mathbf{x}_n), \mathbf{Z}_{\Theta}(\mathbf{x}_n), \mathbf{Z}_{\Theta_2}(\mathbf{x}_n)\right)$, Φ is the prescribed marginal CDF of a standard Gaussian variable, and F_X^{-1} is the inverse CDF of the target marginal PDF of the random field.

2.3. Numerical simulation of polycrystals and simulation parameters

Using the open-source software NEPER [16-17], 500 realizations of a polycrystalline microstructure were numerically simulated, each of which constituted of 1000 equiaxed grains. A voxel-based tessellation approach is used to generate each realization being a 1 μm × 1 μm × 1 μm cube. One of the models along with its grain size statistics is shown in Fig. 3. It should be noticed that the centroid location and the size of each grain in each model differ from each other.
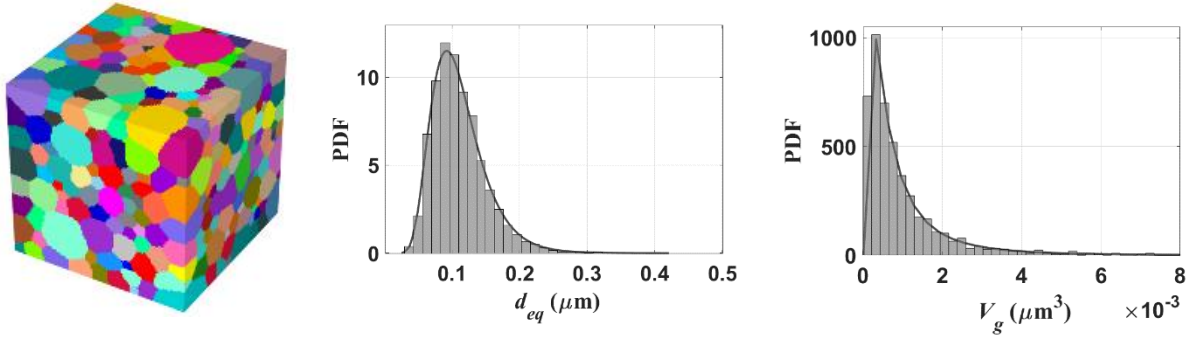

Figure 3 – A realization of a numerically simulated polycrystal using NEPER (left), with PDFs of its equivalent diameter d_{eq} (middle) and that of the grain volumes V_g (right).

Euler angles random fields are then numerically simulated based on the abovementioned sample. The Euclidean norm is used to calculate the distance between two centroids of crystals. We consider a correlation length of three times the average equivalent diameter $\underline{d}_{eq}$ ($\underline{d}_{eq} \approx 0.124$ μm) of aforementioned numerically simulated polycrystals, the NCCFs are 0, the NACFs ($\widehat{R}_{\Theta_1\Theta_1}$, $\widehat{R}_{\Theta\Theta}$ and $\widehat{R}_{\Theta_2\Theta_2}$) of the random Euler angles are supposed to be the same and follow the form of Eq. (6) with the estimated values of l_X:

$$l_X = (l_{\Theta_1}, l_{\Theta}, l_{\Theta_2}) \cong (0.372, 0.372, 0.372) \text{ μm.} \tag{9}$$

Nine cubic materials with different levels of anisotropy are studied, whose average elastic parameters are given in Table 1. Zener anisotropy index $A_Z = 2c_{44}/(c_{11} - c_{12})$ [22] is used to measure the anisotropy level A, which is defined as $A = |1 - A_Z|$. It should be pointed out that for the particular isotropic case, Zener anisotropy index A_Z equals to 1, thus the value of the defined anisotropy level A vanishes. Random elasticity tensors with fluctuation level δ and spatially correlated crystallographic orientations for these materials are simulated using MATLAB.

4

3. Computational framework by using self-consistent method

The so-called self-consistent method was originally proposed by Hershey [8] and Kröner [9] to predict the macroscopic elastic properties for aggregates of crystals. Eshelby's work [3] shows that if uniform strains are applied in far-field of unbounded homogeneous isotropic medium, an ellipsoidal inhomogeneity embedded in this medium would also feel a uniform strain. Based on them, Lubarda [13] gives the expression of the fourth-rank concentration tensor A_{ijkl} for cubic crystals with spherical shape surrounded by isotropic polycrystalline aggregates as:

$$A_{ijkl} = I_{ijkl} + k(\delta_{ij}\delta_{kl} + 2I_{ijkl} - 5T_{ijkl}), \tag{10}$$

wherein I_{ijkl} is the second-rank identity tensor, T_{ijkl} is the random rotation tensor that can be decomposed to the rotation matrices in terms of Euler angles $(\Theta_1, \Theta, \Theta_2)$. Moreover, k is calculated in terms of 3 parameters c_{11}, c_{12} and c_{44}^*:

$$k = \frac{(c_{11} + 2c_{12} + 6c_{44}^*)(c_{11} - c_{12} - 2c_{44}^*)}{3[8c_{44}^{*2} + 9c_{11}c_{44}^* + (c_{11} - c_{12})(c_{11} + 2c_{12})]}, \tag{11}$$

in which c_{44}^* is the positive root of the following cubic equation:

$$8(c_{44}^*)^3 + (5c_{11} + 4c_{12})(c_{44}^*)^2 - c_{44}(7c_{11} - 4c_{12})c_{44}^* - c_{44}(c_{11} - c_{12})(c_{11} + 2c_{12}) = 0. \tag{12}$$

Following Lubarda, self-consistent estimate of elasticity tensor for spherical geometry cubic crystals can be expressed as:

$$C_{ijkl}^{sc} = C_{ijmn}A_{mnkl}, \tag{13}$$

where C_{ijmn} is fourth-rank elasticity tensor of crystal.

The effective stiffness tensor of polycrystals with volume V for N_{real} realizations can thus be calculated using the volume average:

$$\langle C_{ijkl}^{sc,j} \rangle = \frac{1}{V} \int_\Gamma C_{ijkl}^{sc,j}(\mathbf{x}) d^3\mathbf{x}, \qquad j = 1, \dots, N_{real}, \tag{14}$$

where Γ is the cubic domain of definition of each realization. The effective bulk and shear moduli could be subsequently calculated in terms of the corresponding volume averages $\langle C_{ijkl}^{sc,h} \rangle$ for each realization.

4. Numerical results and discussion

The numerical study on the effective elastic properties of nine cubic materials defined in Table 1 has been done. Statistical convergence of first and second-order statistics is investigated on 500 realizations of each material. The convergence criterion is defined as the corresponding error being less than 2 %.
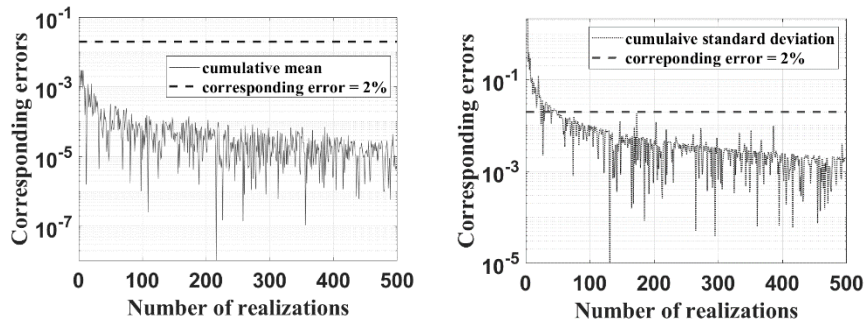

Figure 4 – Corresponding errors of first and second-order statistics of elastic modulus c_{44}^{sc} of α-Fe. The crystallographic orientations are spatially correlated random fields with a fluctuation level $\delta = 0.1$.

Fig. 4 shows that the corresponding errors of the first and second-order statistics of elastic modulus c_{44}^{sc} for α-Fe. The crystallographic orientations here are spatially correlated random fields with a fluctuation level of $\delta = 0.1$. From Fig. 4, it is shown that both the first and second-order statistics converge for 500 realizations. It should be noted that this statistical convergence investigation has also been done on c_{11}^{sc} and c_{12}^{sc} for each material in Table 1 and similar results can be obtained as shown in Fig. 4.
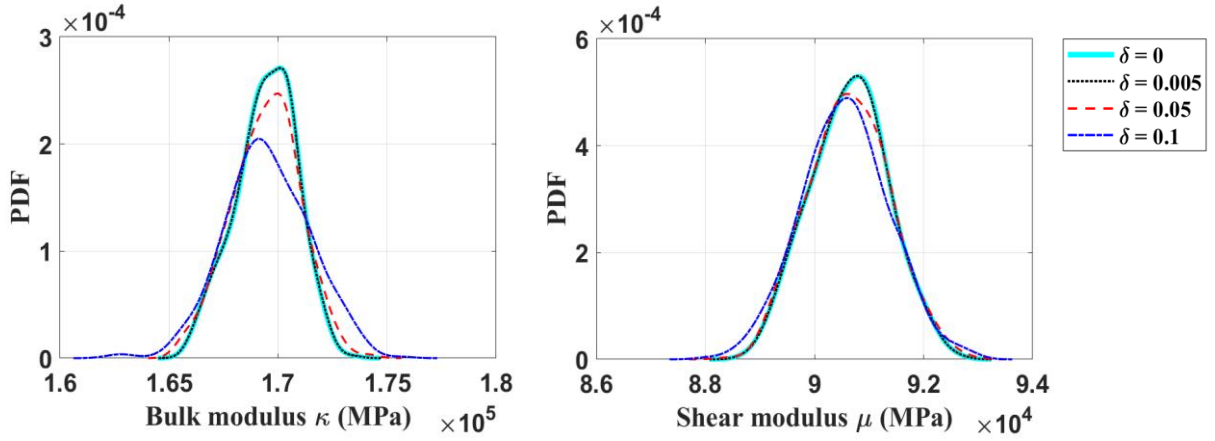

Figure 5 – PDFs of the effective bulk and shear moduli based on 500 realizations of α-Fe polycrystal with different dispersion levels δ. The crystallographic orientations are spatially correlated random fields.

Figure 5 shows, for different dispersion levels δ, the distributions of the effective bulk and shear moduli based on 500 samples of α-Fe. It can be seen that with a higher fluctuation level, the range is wider, together with a higher variation level.

Table 2 – Coefficients of variation of effective bulk and shear moduli of Al, α-Fe and Li for 500 realizations. The crystallographic orientations are spatially correlated random fields with four fluctuation levels.

Name	Coefficient of variation							
	Bulk modulus κ (MPa)				Shear modulus μ (MPa)			
	$\delta = 0$	$\delta = 0.005$	$\delta = 0.05$	$\delta = 0.1$	$\delta = 0$	$\delta = 0.005$	$\delta = 0.05$	$\delta = 0.1$
Al	0.00138	0.00146	0.00468	0.00896	0.00181	0.00181	0.00274	0.00443
α-Fe	0.00816	0.00818	0.00917	0.01152	0.00783	0.00783	0.00815	0.00886
Li	0.01370	0.01372	0.01427	0.01575	0.01924	0.01924	0.01939	0.01975

The cumulative coefficients of variation (cumCoV) of the effective bulk and shear moduli (κ, μ) of these cubic materials have been calculated. Using the bootstrap approach with a resampling size of 10000, 95 % two-sided confidence intervals of the cumCoV of (κ, μ) of α-Fe polycrystals with two fluctuation levels ($\delta = 0.005$ and $\delta = 0.1$) are plotted in Fig. 6. The results show that higher fluctuation levels **δ** result in larger values for the cumCoV of both κ and μ. This tendency could be found in all materials among which we have chosen three cubic materials Al, α-Fe and Li having the lowest, intermediate and the highest anisotropy degrees and the values of their coefficients of variation of the effective bulk and shear moduli are listed in Table 2. From Table 2, a small fluctuation level ($\delta = 0.005$) on elastic tensor of crystals will obviously influence the cumCoV of the effective bulk modulus of the polycrystals. As δ increases, cumCoV of the effective shear modulus is influenced and the value becomes gradually larger.
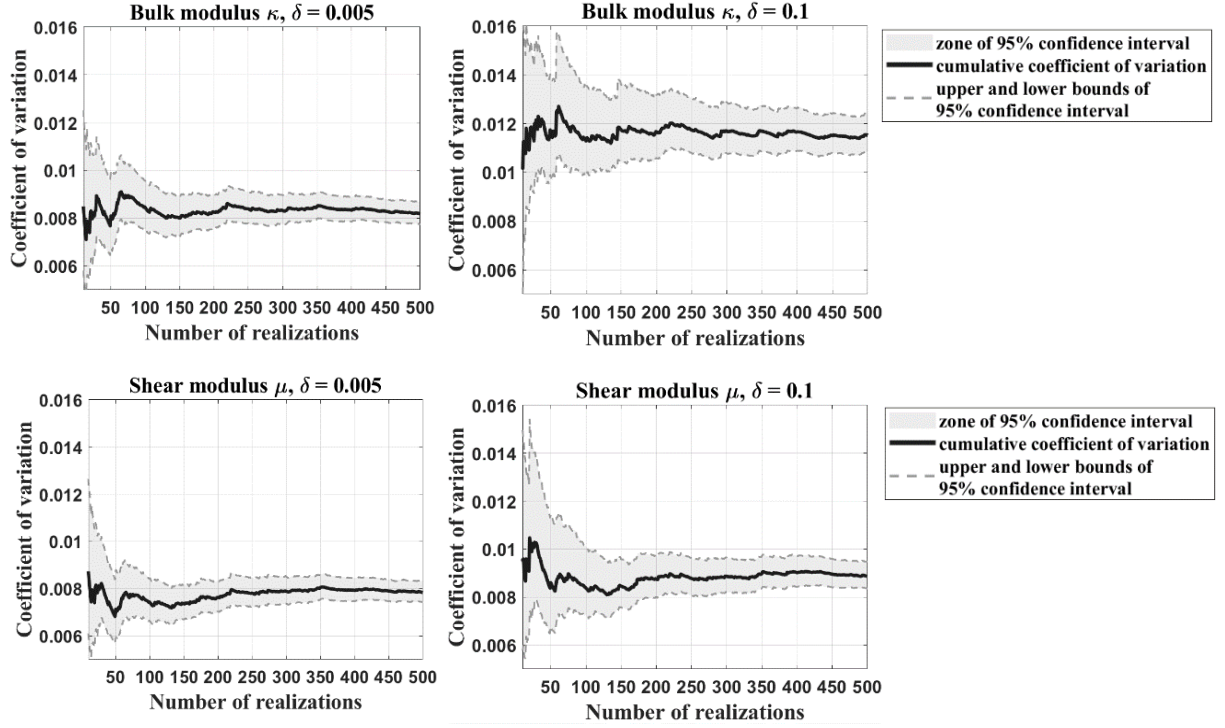
Figure 6 – Coefficient of variation of the effective bulk and shear moduli of α-Fe polycrystals in terms of the realization numbers along with two-sided 95 % confidence intervals. The crystallographic orientations are spatially correlated random fields with two fluctuation levels (δ = 0.005 and δ = 0.1).

Fig. 7 depicts the variation of the coefficient of variation of the effective elastic properties of the materials summarized in Table 1 in terms of the number of realizations, for a fluctuation level of δ = 0.1. The former reveals that higher anisotropy indices imply larger fluctuation levels of the effective properties. For instance, when the elastic parameter c_{44} of the stiffness matrix of Li in its local coordinates has a fluctuation level of δ = 0.1, the corresponding effective bulk and shear moduli will have fluctuation levels of about 1.6 % and 2 %, respectively. This result shows the importance of taking into consideration the variability on the single crystal elastic moduli on our numerical modeling.
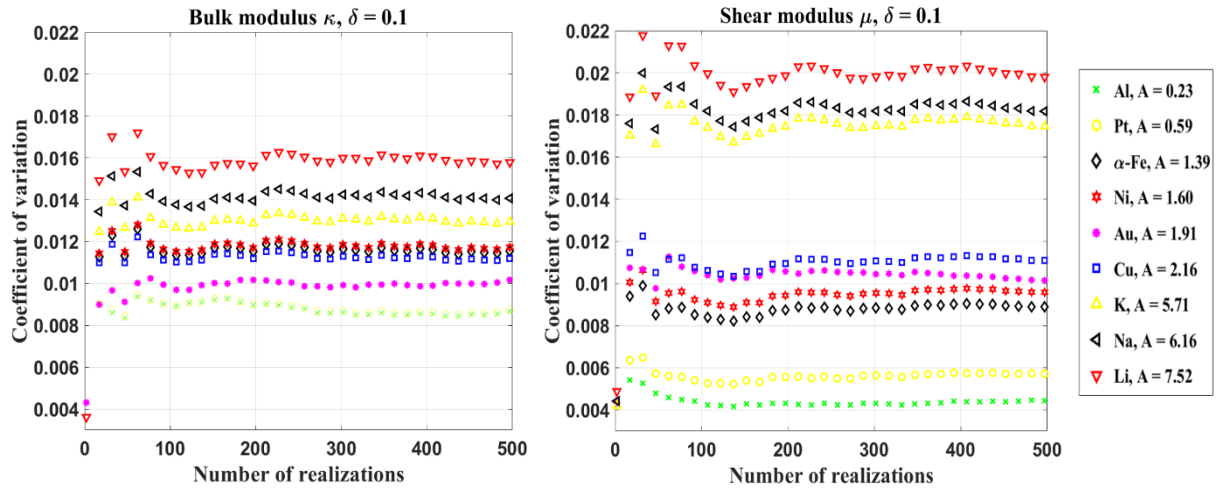

Figure 7 – Coefficient of variation of the effective bulk and shear moduli of nine cubic polycrystals in terms of the realization numbers. The crystallographic orientations are spatially correlated random fields with the fluctuation level δ = 0.1.

5. Conclusion

In this work, random elasticity tensor with a given fluctuation level δ was numerically simulated. By introducing the variabilities on the elastic moduli of grains, numerical models of polycrystals were constructed, whose crystallographic orientations are spatially correlated random fields based on the real sample. The influence of this variability on the statistical parameters of the effective elastic properties of polycrystals for nine different cubic materials was investigated by using the self-consistent method. The results show that even if the single crystal elasticity tensor has a small fluctuation level, it will still have an impact on the distribution of the effective bulk and shear moduli of the polycrystal.

The next step is to use the finite element method to estimate the effective elastic properties of textured materials having any given class of material symmetry.

References

[1] W. Boas, J.K. Mackenzie. *Anisotropy in metals*. Progress in Metal Physics, page 90 - page 120, 1950.

[2] G. Doumenc. *Fabrication additive arc-fil en alliage d'aluminium à durcissement structural AA6061 : relations procédé, microstructures et propriétés mécaniques*. Thèse de doctorat. 2021.

[3] J. D. Eshelby. *The determination of the elastic field of an ellipsoidal inclusion, and related problems*. Proceedings of the Royal Society A, page 376 - page 396, 1957.

[4] A. G. Every, A. K. McCurdy. *Second and higher-order elastic constants*. Springer-Verlag, Berlin, 1992.

[5] E. Goens, E. Schmid. *Über die elastische Anisotropie des Eisens*. Naturwissenschaften, page 520-page 524, 1931.

[6] J. Guilleminot, C. Soize. *On the Statistical Dependence for the Components of Random Elasticity Tensors Exhibiting Material Symmetry Properties*. Journal of Elasticity, page 109 - page 130, 2013.

[7] M. W. Guinan, D. N. Beshers, *Pressure derivatives of the elastic constants of α-iron to 10 kbs*. Journal of Physics and Chemistry of Solids, page 541 - page 549, 1968.

[8] A. V. Hershey. *The elasticity of an isotropic aggregate of anisotropic cubic crystals*. Journal of Applied Mechanics, page 236 - page 240 , 1954.

[9] E. Kröner. *Berechnung der elastischen konstanten des vielkristalls aus den konstanten des einkristalls*. Zeitschrift für Physik, page 504 - page 518, 1958.

[10] H. Ledbetter, S. Kim. *Monocrystal Elastic Constants and Deprived Properties of the Cubic and the Hexagonal Elements*, Handbook of Elastic Properties of Solids, Fluids, and Gases, page 97 - page 106, 2001.

[11] M. Loève. *Probability Theory, Fourth Edition*. Springer-Verlag, New York, 1977.

[12] A. E. Lord, D. N. Beshers. *Elastic Stiffness Coefficients of Iron from 77° to 673°K*. Journal of Applied Physics, page 1620 - page 1623, 1965.

[13] V. A. Lubarda. *New estimates of the third-order elastic constants for isotropic aggregates of cubic crystals*. Journal of the Mechanics and Physics of Solids, page 471 - page 490, 1997.

[14] M. Moakher, A. N. Norris. *The Closest Elastic Tensor of Arbitrary Symmetry to an Elasticity Tensor of Lower Symmetry*. Journal of Elasticity, page 215 - page 263, 2006.

[15] H. Möller, F. Brasse. *Spannungs- und Verzerrungszustand an der Grenzfläche zweier Kristalle*. Arch. Eisenhüttenwesen, page 437 - page 443, 1955.

[16] R. Quey, P. R. Dawson, F. Barbe. *Large-scale 3D random polycrystals for the finite element method: Generation, meshing and remeshing*. Computer Methods in Applied Mechanics and Engineering, page 1729 - page 1745, 2011.

[17] R. Quey, L. Renversade. *Optimal polyhedral description of 3D polycrystals: Method and application to statistical and synchrotron X-ray diffraction data*. Computer Methods in Applied Mechanics and Engineering, page 308 - page 333, 2018.

[18] J. A. Rayne, B. Chandrasekhar. *Elastic Constants of Iron from 4.2 to 300°K*. Physical Review, page 1714 - page 1716, 1961.

[19] C. Soize. *A nonparametric model of random uncertainties on reduced matrix model in structural dynamics*. Probabilistic Engineering Mechanics, page 277 - page 294, 2000.

[20] P. Spanos, R. Ghanem. *Stochastic Finite Elements: A Spectral Approach*. Springer, New York, 1991.

[21] J. Turley, G. Sines. *The anisotropy of Young's modulus, shear modulus and Poisson's ratio in cubic materials*. Journal of Physics D: Applied Physics, page 264 - page 271, 1971.

[22] C. Zener. *Elasticity and Anelasticity of Metals*. University of Chicago Press, Chicago, 1948.